MerTK cleavage limits proresolving mediator biosynthesis and exacerbates tissue inflammation

Bishuang Cai[a,b,c], Edward B. Thorp[d], Amanda C. Doran[a,b,c], Manikandan Subramanian[a,b,c], Brian E. Sansbury[e], Chyuan-Sheng Lin[a,b,c], Matthew Spite[e], Gabrielle Fredman[f,1], and Ira Tabas[a,b,c,1]

[a]Department of Medicine, Columbia University, New York, NY 10032; [b]Department of Pathology and Cell Biology, Columbia University, New York, NY 10032; [c]Department of Physiology, Columbia University, New York, NY 10032; [d]Department of Pathology, Feinberg Cardiovascular Research Institute, Northwestern University, Chicago, IL 60611; [e]Center for Experimental Therapeutics and Reperfusion Injury, Department of Anesthesia, Brigham and Women's Hospital and Harvard Medical School, Boston, MA 02115; and [f]Center for Cardiovascular Sciences, Department of Molecular and Cellular Physiology, Albany Medical College, Albany, NY 12208

The acute inflammatory response requires a coordinated resolution program to prevent excessive inflammation, repair collateral damage, and restore tissue homeostasis, and failure of this response contributes to the pathology of numerous chronic inflammatory diseases. Resolution is mediated in part by long-chain fatty acid-derived lipid mediators called specialized proresolving mediators (SPMs). However, how SPMs are regulated during the inflammatory response, and how this process goes awry in inflammatory diseases, are poorly understood. We now show that signaling through the Mer proto-oncogene tyrosine kinase (MerTK) receptor in cultured macrophages and in sterile inflammation in vivo promotes SPM biosynthesis by a mechanism involving an increase in the cytoplasmic:nuclear ratio of a key SPM biosynthetic enzyme, 5-lipoxygenase. This action of MerTK is linked to the resolution of sterile peritonitis and, after ischemia–reperfusion (I/R) injury, to increased circulating SPMs and decreased remote organ inflammation. MerTK is susceptible to ADAM metallopeptidase domain 17 (ADAM17)-mediated cell-surface cleavage under inflammatory conditions, but the functional significance is not known. We show here that SPM biosynthesis is increased and inflammation resolution is improved in a new mouse model in which endogenous MerTK was replaced with a genetically engineered variant that is cleavage-resistant (Mertk^{CR}). Mertk^{CR} mice also have increased circulating levels of SPMs and less lung injury after I/R. Thus, MerTK cleavage during inflammation limits SPM biosynthesis and the resolution response. These findings contribute to our understanding of how SPM synthesis is regulated during the inflammatory response and suggest new therapeutic avenues to boost resolution in settings where defective resolution promotes disease progression.

MerTK | efferocytosis | inflammation resolution | macrophages | 5-lipoxygenase

The resolution response after acute inflammation is necessary for tissue homeostasis (1, 2), and impaired resolution is an underlying component of several chronic inflammatory diseases, including atherosclerosis and neurodegeneration (3–5). Resolution is an active process involving the production of molecules that signal through specific cell-surface receptors to temper inflammation, enhance efferocytosis, and repair tissue damage without compromising host defense (1, 6–8). Specialized proresolving mediators (SPMs), which are derived from long-chain fatty acids, represent a key family of resolution effectors. Examples include arachidonic acid (AA)-derived lipoxins, like LXA$_4$, and docosahexaenoic acid (DHA)-derived resolvins, such as RvD1 (1, 9, 10). Interestingly, SPMs can promote their own synthesis; for example, RvD1 promotes the biosynthesis of LXA$_4$ via nuclear exclusion of 5-lipoxygenase (5-LOX) (11, 12). Despite these advances, a major gap is the identification of upstream regulators of SPM production.

Mer proto-oncogene tyrosine kinase (MerTK) is a macrophage cell-surface protein that mediates a key process in inflammation resolution, efferocytosis, by interacting with Gas6 or protein S,

which are bridging molecules that bind externalized phosphatidylserine on apoptotic cells (ACs) (13, 14). MerTK engagement triggers AC internalization via cytoskeletal signaling, and it also activates an anti-inflammatory response by suppressing NF-κB (15, 16). As such, MerTK knockout mice develop a lupus-like phenotype in aged mice (17), demonstrate accelerated atherosclerosis in hypercholesterolemic mice due to defective clearance of ACs and heightened inflammation (18, 19), and have increased peritonitis in response to a sterile inflammatory stimulus (20).

Under inflammatory conditions or in the presence of PKC activators, the ectodomain of MerTK is cleaved by the metalloproteinase ADAM17 (21, 22). This process disables MerTK, and the cleavage product, soluble Mer (sol-Mer), may competitively inhibit the interaction of intact MerTK with its ligands (21, 22). Plasma sol-Mer is increased in patients with active systemic lupus erythematosus and rheumatoid arthritis (23, 24), and cell-surface MerTK is lower in macrophages in ADAM17-rich areas in advanced human atherosclerotic lesions (25). However, causation studies are lacking. For example, studies using ADAM17 inhibitors are difficult to interpret in view of its many substrates. In this regard, we recently identified proline-485 as the MerTK cleavage site and showed that cells expressing MerTK lacking residues 483–488 (MerTK$^{\Delta 483-488}$) maintained MerTK-dependent efferocytosis under cleavage-inducing conditions (22).

Significance

Specialized proresolving mediators (SPMs) are lipids that temper inflammation, enhance efferocytosis, and repair tissue damage after inflammation. However, the upstream regulators of SPM production are not completely identified. We show here that Mer proto-oncogene tyrosine kinase (MerTK) signaling in macrophages promotes the production of SPMs both in vitro and in vivo, and thereby contributes to the resolution process. Moreover, inflammation-induced MerTK cleavage can limit this response, as shown by the improvement in resolution in a new MerTK-cleavage resistant mouse model. These findings increase our knowledge of the regulation of SPM biosynthesis and suggest new ideas for improving resolution in chronic inflammatory diseases.

The various actions of MerTK suggest that it may be a critical mediator of the resolution response, and efferocytosis can stimulate SPM formation (26, 27). Therefore, we wondered whether MerTK signaling may be involved in the critical resolution process of SPM biosynthesis and whether cleavage of MerTK might contribute to defective resolution in certain inflammatory settings. We show that MerTK signaling promotes the production of SPMs both in vitro and in vivo by affecting the intracellular localization of 5-LOX and that it contributes to circulating SPMs and limits remote organ damage after ischemia–reperfusion (I/R) injury. Moreover, using a new mouse model in which the endogenous *Mertk* locus has been replaced by one that encodes cleavage-resistant MerTK$^{\Delta 483-488}$ (*Mertk^{CR}*), we show that MerTK cleavage limits resolution in sterile peritonitis and I/R.

Results

MerTK Deficiency Delays Resolution, Decreases Polymorphonuclear Leukocyte Efferocytosis, and Lowers SPM Levels in Sterile Inflammation.

Zymosan-induced peritonitis is a widely used model of sterile inflammation (28). To study the role of MerTK, we injected *Mertk$^{-/-}$* and WT mice with zymosan intraperitoneally and assayed exudate polymorphonuclear leukocytes (PMNs) over time (Fig. 1A). There was a rapid influx of PMNs that peaked at ~8.5×10^6 cells at 12 h
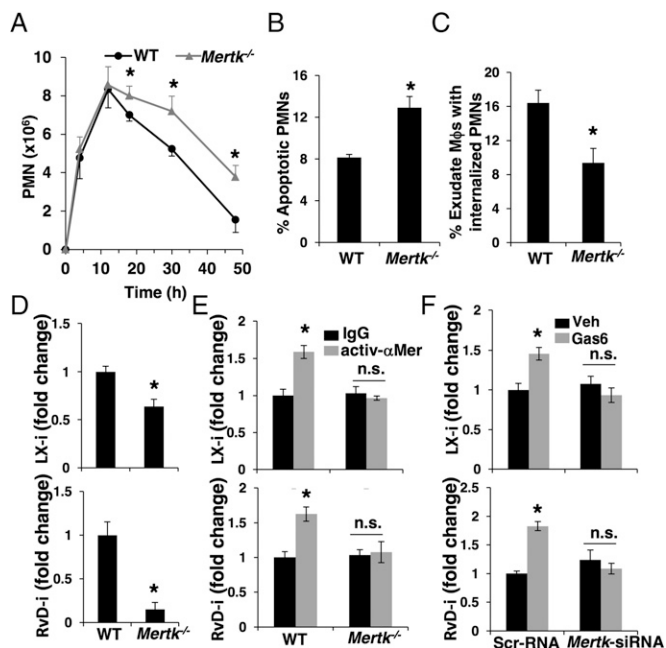
(T_{max}) in both groups. PMNs in both groups then declined, but the decline was delayed in the *Mertk$^{-/-}$* cohort: The decrease to 50% peak value (T_{50}) was ~35 h in WT vs. ~45 h in *Mertk$^{-/-}$*, yielding resolution intervals ($T_{max} - T_{50}$) of ~23 h in WT mice and ~33 h in *Mertk$^{-/-}$* mice. Moreover, the *Mertk$^{-/-}$* exudate showed a significant increase in the percentage of apoptotic PMNs and a significant decrease in the percentage of macrophages with internalized PMNs compared with WT mice (Fig. 1 B and C and Fig. S1 A and B), consistent with defective efferocytosis.

In view of these data, we questioned whether MerTK deficiency somehow suppressed the production of SPMs during resolution. We therefore assayed peritoneal exudates for immunoreactive SPMs using ELISAs and found that mediators recognized by antilipoxin and antiresolvin antibodies were significantly decreased in *Mertk$^{-/-}$* mice (Fig. 1D). We confirmed these overall findings by liquid-chromatography tandem mass spectrometry (LC-MS/MS), first showing distinct groupings of the lipid mediator profile in WT and *Mertk$^{-/-}$* cohorts by partial least squares-discriminant analysis (PLS-DA) and then finding that combined exudate SPMs were lower in the exudates of the *Mertk$^{-/-}$* cohort compared with the WT cohort (Fig. S2 A and B, black and light gray symbols and bars). Neither LTB$_4$, the level of which was very low at this time point, nor combined prostaglandins (PGD$_2$, PGE$_2$, and PGF$_{2\alpha}$) were significantly different between the WT and *Mertk$^{-/-}$* cohorts (Fig. S2 C and D, black and light gray bars). Defective resolution and decreased SPM levels can lead to an imbalance of proresolving vs. proinflammatory cytokines (29). Consistent with this concept, we found that TGF-β was decreased and TNF-α was increased in the peritoneal exudates of zymosan-treated *Mertk$^{-/-}$* mice (Fig. S3A). However, the macrophage phenotype markers cell-surface CD206 and inducible NOS (iNOS) were similar in exudate macrophage from WT vs. *Mertk$^{-/-}$* mice (Fig. S3B, first and second bars).

To examine MerTK-mediated SPM production in vitro, we took advantage of an antibody that specifically activates MerTK signaling (30). We first verified that the antibody stimulates MerTK phosphorylation, which is a measure of MerTK activation (Fig. S4A), and then showed that it increased immunoreactive SPMs in WT macrophages, but not *Mertk$^{-/-}$* macrophages (Fig. 1E). Similar results were found with human macrophages that were incubated with the endogenous MerTK ligand Gas6: Immunoreactive SPM levels were increased in a MerTK-dependent manner (Fig. 1F; documentation of MerTK silencing is shown in Fig. S4B). We then analyzed control vs. Gas6-activated WT and *Mertk$^{-/-}$* murine macrophages for DHA- and AA-derived SPMs by LC-MS/MS and verified that these SPMs were increased by Gas6 in a MerTK-dependent manner (Fig. S4C). In theory, MerTK signaling might increase SPMs by down-regulating the SPM-catabolizing enzyme oxidoreductase 15-hydroxyprostaglandin dehydrogenase (15-PGDH/*Hpgd*), but we found that the expression of *Hpgd* did not change with Gas6 treatment of macrophages (Fig. S4D).

Macrophages from *Mertk$^{\Delta 483-488}$* (*Mertk^{CR}*) Are Resistant to Cleavage and Maintain Efferocytosis in Vitro.

In view of the above findings, we questioned whether MerTK cleavage limits resolution in inflammatory settings. To answer this question, it was necessary to create a precise causation model, which we did by creating a mouse in which the *Mertk* locus was replaced by cleavage-resistant *Mertk$^{\Delta 483-488}$* (*Mertk^{CR}*) (Fig. S5). As part of our initial evaluation, we documented that the percentage of resident peritoneal macrophages in *Mertk^{CR}* mice and the expression of cell-surface MerTK on these macrophages were not significantly different from WT values (Fig. S6 A and B) and that blood and splenic immune cells were also similar in the two cohorts (Fig. S6 C and D).

To assess cleavage resistance, bone marrow-derived macrophages (BMDMs) from *Mertk^{CR}* and WT mice were treated with LPS and then assayed for cell-surface MerTK and media sol-Mer. LPS increased sol-Mer and decreased cell-surface MerTK
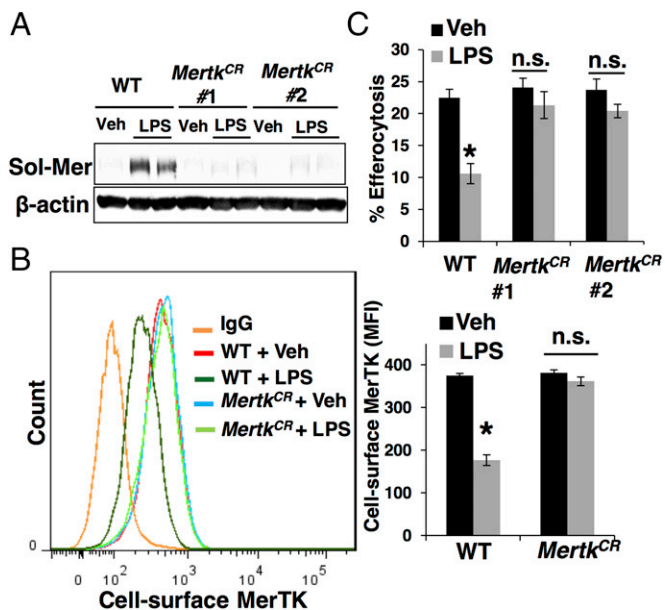

Fig. 1. MerTK deficiency delays resolution, decreases PMN efferocytosis, and lowers SPM levels in sterile peritonitis. (A) WT or *Mertk$^{-/-}$* mice were injected intraperitoneally with 1 mg of zymosan per mouse, and PMNs in the exudate were counted at the indicated times after zymosan injection. (B) Exudate leukocytes at the 30-h time point were costained with annexin V (apoptosis) and anti-Ly6G antibody (PMNs), and the percent of annexin V$^+$ PMNs was detected by flow cytometry. (C) To assess efferocytosis, 30-h exudate leukocytes were first stained with anti-F4/80 antibody, permeabilized and stained for Ly6G, and then analyzed by flow cytometry for F4/80$^+$Ly6G$^+$ cells among total F4/80$^+$ cells. Mφs, macrophages. (D) Exudates were assayed for relative levels of immunoreactive (i) SPMs by LXA$_4$ and RvD1 ELISAs, noted as LX-i and RvD-i, respectively. (E) BMDMs were treated for 1 h with MerTK-activating antibody (activ-αMer) or control IgG, and the media were assayed for relative LX-i and RvD-i, as described in D. (F) Human monocyte-derived macrophages were treated with scrambled (Scr) RNA or siRNA against *Mertk* and then treated for 1 h with vehicle control or human Gas6. The media were assayed for relative LX-i and RvD-i as in D. *P < 0.05 [vs. WT (mean ± SEM, n = 4 mice per group; A–D); and vs. IgG or vehicle control (mean ± SEM, n = 3 experiments; E and F)]; n.s., not significant.

Fig. 2. $Mertk^{CR}$ macrophages are resistant to cleavage and maintain efferocytosis under inflammatory conditions in vitro. (*A* and *B*) BMDMs from a WT mouse or two different $Mertk^{CR}$ mice were incubated for 2 h with 50 ng/mL LPS or vehicle control (Veh). The media were assayed for sol-Mer by immunoblot (*A*), and the cells were assayed for cell-surface MerTK by flow cytometry (*B*); flow data and quantified mean fluorescence intensity (MFI) data are shown. (*C*) BMDMs were treated as in *A* and then incubated for 1 h with Calcein Green-labeled apoptotic Jurkat cells. The percent of total BMDMs with internalized labeled ACs was quantified by analysis of fluorescence microscopy images. *$P < 0.001$ (vs. Veh; mean $\pm$ SEM, $n = 3$ experiments); n.s., not significant.

in WT macrophages, but these effects were largely absent with $Mertk^{CR}$ macrophages (Fig. 2 *A* and *B*; positive control for LPS is shown in Fig. S7*A*). Similar results were seen by using the ADAM17 activator phorbol 12-myristate 13-acetate (PMA) (22) (Fig. S7 *B* and *C*). To assess MerTK function, BMDMs from WT or $Mertk^{CR}$ mice were incubated with apoptotic Jurkat cells in the absence or presence of LPS. Under control conditions, efferocytosis in WT and $Mertk^{CR}$ macrophages was similar, but whereas LPS reduced efferocytosis in WT macrophages, it was maintained in $Mertk^{CR}$ macrophages (Fig. 2*C*). These data validate the $Mertk^{CR}$ mouse model for testing the functional consequences of MerTK cleavage in vivo.

Resolution of Sterile Peritonitis Is Improved in $Mertk^{CR}$ Mice. To test the hypothesis that MerTK cleavage compromises resolution, we compared WT and $Mertk^{CR}$ mice using the zymosan peritonitis model. The data show a marked decrease in PMNs at the 30-h time point in $Mertk^{CR}$ vs. WT mice, with no change in the peak PMN response (Fig. 3*A*), indicative of a specific improvement in the resolution response. By using the parameters described above, the resolution interval was improved approximately two-fold in the $Mertk^{CR}$ mice (~13 vs. 24 h). This improvement was associated with a marked decrease in exudate sol-Mer and an increase in cell-surface MerTK on exudate macrophages (Fig. 3*B*). Sol-Mer in the exudate was likely from macrophages, because neither exudate nor blood PMNs express MerTK (Fig. S8). Efferocytosis was improved in $Mertk^{CR}$ exudate, as indicated by fewer cell-free apoptotic PMNs and more macrophage-internalized PMNs (Fig. 3 *C* and *D* and Fig. S1 *C* and *D*). Most importantly in terms of the role of MerTK in SPM synthesis, $Mertk^{CR}$ exudate had increased immunoreactive SPMs (Fig. 3*E*), and this overall trend was confirmed by LC-MS/MS, which also showed distinct grouping of the $Mertk^{CR}$ cohort by PLS-DA (Fig. S2 *A* and *B*). As with the

$Mertk^{-/-}$ cohort, there were no significant differences or LTB$_4$ or combined prostaglandins (Fig. S2 *C* and *D*). Moreover, the exudate of the $Mertk^{CR}$ cohort showed an increase in TGF-β and a decrease in TNF-α—i.e., opposite, as predicted, from the direction the $Mertk^{-/-}$ exudate (Fig. S3*C*) and consistent with the previous finding that SPMs can increase exudate TGF-β levels in zymosan peritonitis (28). Consistent with the $Mertk^{-/-}$ data (above), cell-surface CD206 and iNOS were similar in exudate macrophage from WT vs. $Mertk^{CR}$ mice (Fig. S3*B*).

To further probe the relationship between MerTK cleavage and SPMs, we tested the effect of MerTK-activating antibody on macrophages treated with or without the cleavage inducer PMA. Under control conditions, the antibody was able to boost mediators recognized by the antilipoxin ELISA equally well in WT and $Mertk^{CR}$ macrophages (Fig. 3*F*, first two pairs of bars). With PMA, anti-MerTK was unable to increase these mediators in WT macrophages, but it was able to increase them in $Mertk^{CR}$
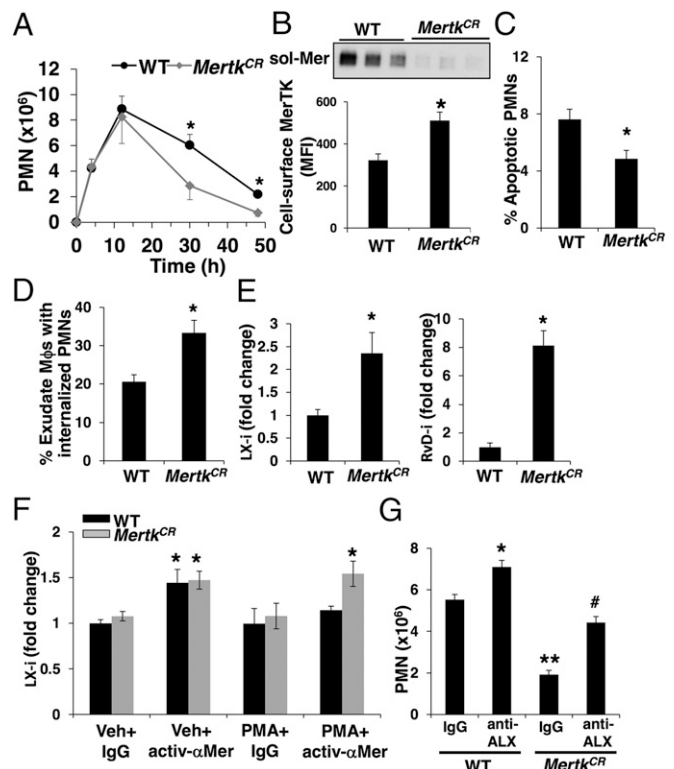

Fig. 3. Resolution of sterile peritonitis is improved in $Mertk^{CR}$ mice. (*A*) WT or $Mertk^{CR}$ mice were injected intraperitoneally with zymosan as in Fig 1, and exudate PMN were quantified at the indicated times after zymosan injection. (*B*) A portion of the peritoneal exudate harvested at 30 h was assayed for sol-Mer by immunoblot, and another portion was costained with anti-F4/80 and -MerTK, followed by flow-cytometric quantification of cell-surface MerTK on F4/80$^+$ cells. (*C* and *D*) Apoptotic PMNs and efferocytosis of PMNs by macrophages in the 30-h exudate were determined as in Fig. 1 *B* and *C*. (*E*) Relative levels of exudate LX-i and RvD-i were measured at 30 h by ELISA. (*G*) BMDMs were treated with 50 nM PMA or vehicle control for 2 h. The cells were then incubated for 1 h with MerTK-activating antibody (activ-αMer) or IgG, and the media were assayed for relative LX-i by ELISA. (*G*) As in *A*, but at 20 h after zymosan, the mice were injected intraperitoneally with blocking antibody against ALX or IgG control, and then exudate PMNs were quantified at 30 h after zymosan. *$P < 0.05$ [vs. WT (mean $\pm$ SEM, $n = 4$ mice per group; *A*–*E*)]. In *F*, bars with asterisks are statistically the same among each other and different from all other bars at $P < 0.05$ (mean $\pm$ SEM, $n = 3$ experiments); for *G*, different symbols indicate values that are statistically different from each other and from IgG control at $P < 0.05$ (mean $\pm$ SEM, $n = 4$ mice per group).
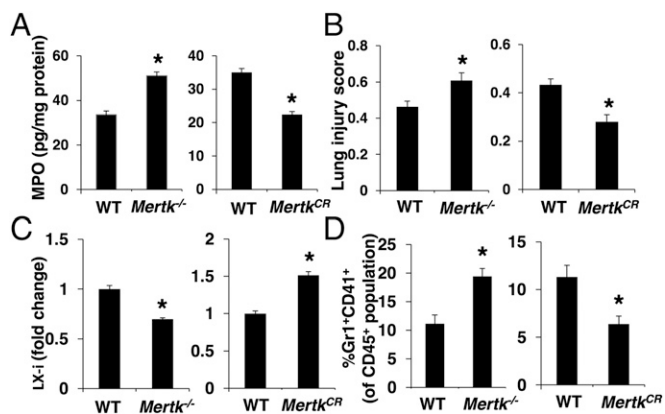
Fig. 4. I/R-induced lung damage is increased in $Mertk^{-/-}$ mice and decreased in $Mertk^{CR}$ mice, with reciprocal changes in plasma LX-i. $Mertk^{-/-}$, $Mertk^{CR}$, or littermate WT mice were subjected to 60-min bilateral hindlimb ischemia followed by 90-min reperfusion. (A) Lung extracts were assayed for MPO content by ELISA (sham values for WT, $Mertk^{-/-}$, and $Mertk^{CR}$ were 6.2, 7.7, and 5.5 pg/mg protein, respectively). (B) Perfused and fixed lungs were scored for lung injury as described in *Materials and Methods*. Representative images are shown in Fig. S9. Sham values for WT, $Mertk^{-/-}$, and $Mertk^{CR}$ were 0.17, 0.176, and 0.148, respectively. (C) Plasma was assayed for relative LX-i by ELISA (sham values for WT, $Mertk^{-/-}$, and $Mertk^{CR}$ were 137.5, 108.8, and 106.2 pg/mL, respectively). (D) Whole blood was immunostained for CD45, Gr1, and CD41, and the percent of $Gr1^+CD41^+$ cells (PMN-platelet aggregates) among total $CD45^+$ cells was quantified by flow cytometry (sham values for WT, $Mertk^{-/-}$, and $Mertk^{CR}$ were 1.5%, 1.3%, and 1.6%, respectively). *$P < 0.002$ (mean ± SEM, $n = 6$–10 mice per group).

macrophages (Fig. 3F, last two pairs of bars). Thus, MerTK cleavage limits the ability of MerTK activation to boost mediators recognized by the antilipoxin under cleavage conditions.

To determine whether the increase in SPMs was linked to the improvement in resolution in $Mertk^{CR}$ mice, we prevented SPM action by intraperitoneal injection of a blocking antibody against the common RvD1/LXA$_4$ receptor ALX/FPR2. This treatment prevented the proresolving benefit of $Mertk^{CR}$, as indicated by a twofold elevation in PMNs at 30 h (Fig. 3G). Thus, in sterile peritonitis, MerTK cleavage limits its proresolving actions, including efferocytosis and SPM synthesis.

I/R-Induced Lung Damage Is Increased in $Mertk^{-/-}$ Mice and Decreased in $Mertk^{CR}$ Mice, with Reciprocal Changes in Immunoreactive Plasma LX. To explore the role of MerTK in a tissue injury model, we used a hindlimb I/R model, where reperfusion injury triggers a systemic inflammatory response leading to remote organ (lung) injury (31, 32). The data show that post-I/R lung myeloperoxidase (MPO), a marker of PMN infiltration (33), and lung injury, quantified as described by Matute-Bello et al. (34), were increased in $Mertk^{-/-}$ mice and decreased in $Mertk^{CR}$ mice (Fig. 4 A and B and Fig. S9A). Moreover, immunoreactive plasma LX (LX-i) was significantly decreased in $Mertk^{-/-}$ mice and increased in $Mertk^{CR}$ mice (Fig. 4C), which was associated with a decrease in TGF-β and increase in TNF-α in $Mertk^{-/-}$ mice and an increase in TGF-β and a decrease in TNF-α in $Mertk^{CR}$ mice (Fig. S9B). SPMs have been shown to attenuate platelet–PMN interaction and reduce I/R-induced lung injury (32). In this context, we found that platelet–PMN aggregates were substantially enhanced in $Mertk^{-/-}$ mice and reduced in $Mertk^{CR}$ mice (Fig. 4D). These data further substantiate the proresolving role of MerTK and its compromise by MerTK cleavage.

MerTK-Induced SPM Production Involves an Increase in the Cytoplasmic: Nuclear Ratio of 5-LOX. A previous study reported that incubation of macrophages with ACs increased LXA$_4$ in a TGF-β–dependent

manner (35). However, the AC receptors, mechanisms, and significance in vivo were not explored, and we found that the MerTK-mediated increase in LX-i was not inhibited by treating the cells with the TGF-β receptor type I/II kinase inhibitor LY2109761 (Fig. S10A); as a positive control for LY2109761, we show that it lowers the TGF-β signaling intermediate p-SMAD2 (Fig. S10A, Inset). We next focused on the regulation of SPM vs. leukotriene synthesis by the cellular location and phosphorylation of 5-LOX, because cytoplasmic 5-LOX, in contrast to nuclear p-Ser271–5-LOX, promotes SPM synthesis (36). For example, ALX activation by SPMs in macrophages can promote cytoplasmic 5-LOX and LXA$_4$ synthesis (11). To determine whether this mechanism is used by MerTK to promote SPM biosynthesis, we treated macrophages with MerTK-activating antibody or control IgG and analyzed the intracellular localization of 5-LOX by confocal immunofluorescence microscopy. In MerTK-activated macrophages, there was an approximately twofold increase in the cytoplasmic:nuclear ratio of 5-LOX (Fig. 5A). Similar results were obtained by using ACs to activate MerTK (Fig. 5B). To assay p-Ser271–5-LOX, we used human macrophages due to antibody specificity and found that activation of MerTK by its ligand Gas6 lowered p-Ser271–5-LOX (Fig. 5C) and decreased the activity
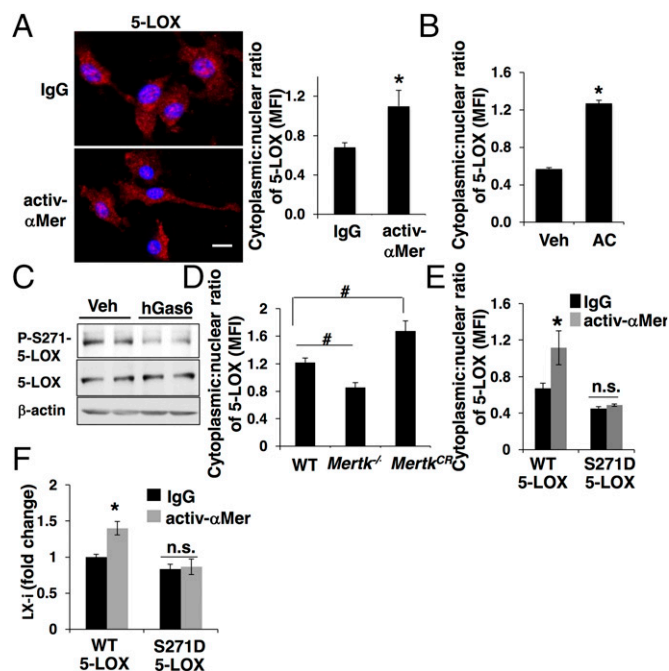
Fig. 5. MerTK promotes SPM production via an increase in the cytoplasmic: nuclear ratio of 5-LOX. (A) BMDMs were treated for 1 h with activ-αMer or control IgG. The cells were then fixed, permeabilized, and immunostained for 5-LOX, with nuclear DAPI costain. (Scale bar, 10 μm.) The cytoplasmic: nuclear ratio of 5-LOX was quantified from confocal immunofluorescence images. (B) Similar to A, except apoptotic Jurkat cells were used instead of activating antibody. (C) Human monocyte-derived macrophages were treated for 1 h with vehicle control (Veh) or human Gas6 and then immunoblotted for p-Ser271–5-LOX and total 5-LOX. (D) WT, $Mertk^{-/-}$, or $Mertk^{CR}$ mice were injected intraperitoneally with 1 mg of zymosan per mouse, and 30 h later, exudate macrophages were assayed for cytoplasmic:nuclear ratio of 5-LOX. (E) BMDMs from $Alox5^{-/-}$ mice were transfected with plasmids encoding WT 5-LOX or S271D–5-LOX and then incubated with MerTK-activating antibody for 1 h. The cytoplasmic:nuclear ratio of 5-LOX was quantified from confocal immunofluorescence images. (F) BMDMs from $Alox5^{-/-}$ mice were transfected with plasmids encoding WT 5-LOX or S271D–5-LOX and then incubated with activ-αMer for 1 h. The media were assayed for relative LX-i by ELISA. (A and B) *$P < 0.05$ vs. IgG (mean ± SEM, $n = 3$ experiments); (D) #$P < 0.05$ vs. WT (mean ± SEM, $n = 4$ mice/group); and (E) *$P < 0.05$ vs. all other groups (mean ± SEM, $n = 3$ experiments).

of the 5-LOX kinase MK2 (37) (Fig. S10B). Moreover, Gas6 increased cytosolic 5-LOX and decreased nuclear 5-LOX (Fig. S10C). In vivo, the cytoplasmic:nuclear 5-LOX ratio in exudate macrophages 30 h after intraperitoneal zymosan was decreased in $Mertk^{-/-}$ and increased in $Mertk^{CR}$ mice vs. WT mice (Fig. 5D).

To examine causation, we transfected macrophages lacking 5-LOX ($Alox5^{-/-}$) with either WT $Alox5$ or S271D-mutant $Alox5$, which mimics p-5-LOX and promotes its nuclear retention (11). In contrast to the case with WT 5-LOX macrophages, MerTK activation was unable to increase the cytoplasmic:nuclear 5-LOX ratio or LX-i in S271D 5-LOX macrophages (Fig. 5 E and F). These combined data support a model in which MerTK activation increases the ratio of cytoplasmic-to-nuclear 5-LOX and decreases p-S271–5-LOX, which leads to increased production of SPMs.

Discussion

Tyro3-Axl-MerTK (TAM) receptors on myeloid cells, including MerTK, act as a fascinating bridge between two key resolution functions, efferocytosis and suppression of inflammation (38). In particular, MerTK not only mediates efferocytosis, but also triggers signaling responses that dampen inflammation (14, 30, 39–45). We now add SPM synthesis to MerTK's repertoire of proresolving functions. In this context, understanding the regulation of MerTK is a critical issue, with most studies focusing on its transcriptional induction (e.g., by glucocorticoids, LXR, and ERK5) (46–48). The discovery of ADAM17-induced MerTK cleavage raised the possibility of a posttranscriptional mechanism (21, 22), but in vivo proof was lacking because currently available tools (e.g., ADAM17 inhibitors) are nonspecific. By creating a mouse with a specific defect in MerTK cleavage, we now show that this mode of MerTK regulation plays a critical role in efferocytosis and SPM synthesis in inflammatory settings.

A previous study found that $Mertk^{-/-}$ mice had a higher peak of PMNs in response to intraperitoneal zymosan than WT mice (20). In contrast, we found a specific defect in the resolution phase in $Mertk^{-/-}$ mice and specific improvement in resolution in $Mertk^{CR}$ mice—both without any change in peak PMN response. Of note, our peritonitis experiments were conducted in C57BL/6J mice, with validation using a tissue-injury model and with pathway verification in human macrophages. In contrast, the previous study used BALB/c mice, which are more Th2-dominant, have different responses to both sterile and infectious insults, and demonstrate a less robust capacity to initiate tissue repair (49, 50).

A fascinating issue that arises from the findings herein is whether MerTK cleavage has a physiologic role. In the initial phases of the host defense response, robust inflammation is advantageous for both pathogen neutralization and as a trigger for the subsequent resolution response (51). If one considers the larger picture of the ADAM17-cleavage program, including the production of TNF-α (52), early cleavage of MerTK may promote robust inflammation by temporarily delaying the production of SPMs. The compromise in efferocytosis would not be detrimental at this stage, because it would be before PMN apoptosis. Then, when the resolution response is needed and ACs begin to appear, ADAM17 activity would diminish, and the resulting increase in MerTK would promote both resolution and efferocytosis. Whether $Mertk^{CR}$ mice have a disadvantage in certain types of acute infectious settings remains to be determined, but the many functions of ADAM17 that are unperturbed in these mice may prevent this from happening.

In summary, we show that activation of MerTK can trigger the formation of SPMs and promote resolution in vivo and that cleavage of MerTK during inflammation limits these effects. These findings suggest that therapeutic strategies that prevent MerTK cleavage may be particularly beneficial for inflammatory diseases characterized by excessive MerTK cleavage and driven by defective resolution.

Materials and Methods

Zymosan A-Induced Peritonitis. The 8- to 10-wk-old C57BL/6J mice were injected intraperitoneally with 1 mg of zymosan (Sigma) per mouse, and peritoneal exudates were collected at the indicated time intervals at the time of death (28). To block ALX, mice were injected intraperitoneally at 20 h after zymosan with 100 μg per mouse anti-ALX antibody (Santa Cruz Biotechnology). All procedures were conducted in accordance with the Columbia University Standing Committee on Animals guidelines for animal care.

Hindlimb I/R. Hindlimbs were ligated in 10-wk-old mice with no. 16 rubber bands (32) and then removed after 1 h. The mice were killed 90 min later, and whole blood was collected by ventricular puncture using 1-mL syringes precoated with citrate dextrose solution. The lungs were removed and snap-frozen in liquid nitrogen for MPO assay. To score lung injury, lungs were perfused and fixed in 10% (vol/vol) formalin, followed by paraffin embedding, sectioning, and hematoxylin and eosin staining. The sections were examined for five features—PMNs in the alveolar space, the interstitial space, hyaline membranes, proteinaceous debris filling the airspaces, and alveolar septal thickening; this information was used to calculate a lung injury score as described by Matute-Bello et al. (34).

Quantification of Lung MPO. The left upper lung lobe from each mouse was thawed and trimmed to an approximate wet weight of 0.3 mg and then placed in a 2-mL flat-bottom microcentrifuge tube containing 450 μL of ice-cold RIPA buffer (Santa Cruz Biotechnology) with 1× Halt Protease Inhibitor Mixture (Thermo Scientific). The tissue was homogenized on ice by using a hand-held homogenizer, and then centrifuged at $20,000 \times g$ for 10 min. The supernatant fractions were transferred to clean tubes, and MPO was quantified in 50-μL aliquots, in duplicate, using an R&D ELISA kit, per the manufacturer's instructions.

Assay of Sol-Mer. BMDMs were incubated for 2 h in 500 μL of serum-free medium alone or containing 50 ng/mL LPS (*Escherichia coli* 0111:B4; Sigma-Aldrich) or 50 nM PMA (Sigma-Aldrich). The media were collected, concentrated 10-fold with ultracentrifugal filters (10,000 molecular weight cut-off; Amicon), lysed with 4× Laemmli sample buffer, and subjected to SDS-polyacrylamide gel electrophoresis and immunoblot analysis.

Treatment of Macrophages with Gas6. Macrophages were treated with 10 nM γ-carboxylated Gas6 for 1 h, which was added as conditioned medium harvested from Gas6-transfected HEK293-6E cells, as described (53). Conditioned medium from nontransfected HEK293 cells served as the control and is referred to in the figures as "vehicle." Both control and Gas6-conditioned medium were free of SPMs as measured by SPM ELISA.

SPM ELISA Assays. Macrophages were suspended at a concentration of 3×10^6 cells per 300 μL in Dulbecco's PBS containing calcium and magnesium and then incubated for 1 h at 37 °C with 5 nM MerTK-activating antibody (R&D, AF591) vs. control IgG, or vehicle control vs. recombinant γ-carboxylated Gas6. The macrophage media were then harvested for analysis by the Neogen LXA₄ ELISA kit, which has the following cross-reactivities of ≥0.1% according to the manufacturer: 15-epi-LXA₄ (24%), 5(S),6(R)-DiHETE (5%), LXB₄ (1%), and 15-HETE (0.1%); or they were analyzed by the Cayman RvD1 ELISA kit, with cross-reactivities to 5(S),6(R)-LXA₄ (20%), 17(R)-RvD1 (4.2%), and 10(S),17(S)-DiHdoHE (0.7%). We refer to the former as LX-i and the latter as RvD-i, where "i" stands for "immunoreactive." The data are reported as fold change in the experimental group relative to IgG or vehicle control, which was set at 1.0. Similar analyses were conducted on peritoneal exudates for the zymosan experiments and plasma for the I/R experiments. In all cases, the 50 μL of sample, with plasma diluted 1:3, was assayed per the manufacturer's instructions.

Statistics. Student t test or one-way ANOVA with post hoc Tukey tests was used to determine significance. All error bars represent SEM.

IMMUNOLOGY AND INFLAMMATION

1. Serhan CN (2014) Pro-resolving lipid mediators are leads for resolution physiology. *Nature* 510(7503):92–101.
2. Medzhitov R (2010) Inflammation 2010: New adventures of an old flame. *Cell* 140(6):771–776.
3. Nathan C, Ding A (2010) Nonresolving inflammation. *Cell* 140(6):871–882.
4. Tabas I, Glass CK (2013) Anti-inflammatory therapy in chronic disease: Challenges and opportunities. *Science* 339(6116):166–172.
5. Viola J, Soehnlein O (2015) Atherosclerosis—A matter of unresolved inflammation. *Semin Immunol* 27(3):184–193.
6. Perretti M, D'Acquisto F (2009) Annexin A1 and glucocorticoids as effectors of the resolution of inflammation. *Nat Rev Immunol* 9(1):62–70.
7. Wallace JL, Ianaro A, Flannigan KL, Cirino G (2015) Gaseous mediators in resolution of inflammation. *Semin Immunol* 27(3):227–233.
8. Buckley CD, Gilroy DW, Serhan CN (2014) Proresolving lipid mediators and mechanisms in the resolution of acute inflammation. *Immunity* 40(3):315–327.
9. Serhan CN, et al. (2002) Resolvins: A family of bioactive products of omega-3 fatty acid transformation circuits initiated by aspirin treatment that counter proinflammation signals. *J Exp Med* 196(8):1025–1037.
10. Serhan CN, Hamberg M, Samuelsson B (1984) Lipoxins: Novel series of biologically active compounds formed from arachidonic acid in human leukocytes. *Proc Natl Acad Sci USA* 81(17):5335–5339.
11. Fredman G, et al. (2014) Resolvin D1 limits 5-lipoxygenase nuclear localization and leukotriene B4 synthesis by inhibiting a calcium-activated kinase pathway. *Proc Natl Acad Sci USA* 111(40):14530–14535.
12. Norling LV, Dalli J, Flower RJ, Serhan CN, Perretti M (2012) Resolvin D1 limits polymorphonuclear leukocyte recruitment to inflammatory loci: Receptor-dependent actions. *Arterioscler Thromb Vasc Biol* 32(8):1970–1978.
13. Lemke G, Burstyn-Cohen T (2010) TAM receptors and the clearance of apoptotic cells. *Ann N Y Acad Sci* 1209:23–29.
14. Lemke G (2013) Biology of the TAM receptors. *Cold Spring Harb Perspect Biol* 5(11):a009076.
15. Lee YJ, et al. (2012) Inhibiting Mer receptor tyrosine kinase suppresses STAT1, SOCS1/3, and NF-κB activation and enhances inflammatory responses in lipopolysaccharide-induced acute lung injury. *J Leukoc Biol* 91(6):921–932.
16. Choi JY, et al. (2013) Upregulation of Mer receptor tyrosine kinase signaling attenuated lipopolysaccharide-induced lung inflammation. *J Pharmacol Exp Ther* 344(2):447–458.
17. Cohen PL, et al. (2002) Delayed apoptotic cell clearance and lupus-like autoimmunity in mice lacking the c-mer membrane tyrosine kinase. *J Exp Med* 196(1):135–140.
18. Thorp E, Cui D, Schrijvers DM, Kuriakose G, Tabas I (2008) Mertk receptor mutation reduces efferocytosis efficiency and promotes apoptotic cell accumulation and plaque necrosis in atherosclerotic lesions of apoe-/- mice. *Arterioscler Thromb Vasc Biol* 28(8):1421–1428.
19. Ait-Oufella H, et al. (2008) Defective mer receptor tyrosine kinase signaling in bone marrow cells promotes apoptotic cell accumulation and accelerates atherosclerosis. *Arterioscler Thromb Vasc Biol* 28(8):1429–1431.
20. Choi JY, et al. (2015) Mer signaling increases the abundance of the transcription factor LXR to promote the resolution of acute sterile inflammation. *Sci Signal* 8(365):ra21.
21. Sather S, et al. (2007) A soluble form of the Mer receptor tyrosine kinase inhibits macrophage clearance of apoptotic cells and platelet aggregation. *Blood* 109(3):1026–1033.
22. Thorp E, et al. (2011) Shedding of the Mer tyrosine kinase receptor is mediated by ADAM17 protein through a pathway involving reactive oxygen species, protein kinase Cδ, and p38 mitogen-activated protein kinase (MAPK). *J Biol Chem* 286(38):33335–33344.
23. Wu J, et al. (2011) Increased plasma levels of the soluble Mer tyrosine kinase receptor in systemic lupus erythematosus relate to disease activity and nephritis. *Arthritis Res Ther* 13(2):R62.
24. Zizzo G, Guerrieri J, Dittman LM, Merrill JT, Cohen PL (2013) Circulating levels of soluble MER in lupus reflect M2c activation of monocytes/macrophages, autoantibody specificities and disease activity. *Arthritis Res Ther* 15(6):R212.
25. Garbin U, et al. (2013) Expansion of necrotic core and shedding of Mertk receptor in human carotid plaques: A role for oxidized polyunsaturated fatty acids? *Cardiovasc Res* 97(1):125–133.
26. Schwab JM, Chiang N, Arita M, Serhan CN (2007) Resolvin E1 and protectin D1 activate inflammation-resolution programmes. *Nature* 447(7146):869–874.
27. Dalli J, Serhan CN (2012) Specific lipid mediator signatures of human phagocytes: Microparticles stimulate macrophage efferocytosis and pro-resolving mediators. *Blood* 120(15):e60–e72.
28. Bannenberg GL, et al. (2005) Molecular circuits of resolution: Formation and actions of resolvins and protectins. *J Immunol* 174(7):4345–4355.
29. Serhan CN, Chiang N, Van Dyke TE (2008) Resolving inflammation: Dual anti-inflammatory and pro-resolution lipid mediators. *Nat Rev Immunol* 8(5):349–361.
30. Zagórska A, Través PG, Lew ED, Dransfield I, Lemke G (2014) Diversification of TAM receptor tyrosine kinase function. *Nat Immunol* 15(10):920–928.
31. Yassin MM, Harkin DW, Barros D'Sa AA, Halliday MI, Rowlands BJ (2002) Lower limb ischemia-reperfusion injury triggers a systemic inflammatory response and multiple organ dysfunction. *World J Surg* 26(1):115–121.
32. Shinohara M, et al. (2014) Cell-cell interactions and bronchoconstrictor eicosanoid reduction with inhaled carbon monoxide and resolvin D1. *Am J Physiol Lung Cell Mol Physiol* 307(10):L746–L757.
33. McCabe AJ, Dowhy M, Holm BA, Glick PL (2001) Myeloperoxidase activity as a lung injury marker in the lamb model of congenital diaphragmatic hernia. *J Pediatr Surg* 36(2):334–337.
34. Matute-Bello G, et al.; Acute Lung Injury in Animals Study Group (2011) An official American Thoracic Society workshop report: Features and measurements of experimental acute lung injury in animals. *Am J Respir Cell Mol Biol* 44(5):725–738.
35. Freire-de-Lima CG, et al. (2006) Apoptotic cells, through transforming growth factor-beta, coordinately induce anti-inflammatory and suppress pro-inflammatory eicosanoid and NO synthesis in murine macrophages. *J Biol Chem* 281(50):38376–38384.
36. Rådmark O, Samuelsson B (2005) Regulation of 5-lipoxygenase enzyme activity. *Biochem Biophys Res Commun* 338(1):102–110.
37. Werz O, Szellas D, Steinhilber D, Rådmark O (2002) Arachidonic acid promotes phosphorylation of 5-lipoxygenase at Ser-271 by MAPK-activated protein kinase 2 (MK2). *J Biol Chem* 277(17):14793–14800.
38. Rothlin CV, Carrera-Silva EA, Bosurgi L, Ghosh S (2015) TAM receptor signaling in immune homeostasis. *Annu Rev Immunol* 33:355–391.
39. Scott RS, et al. (2001) Phagocytosis and clearance of apoptotic cells is mediated by MER. *Nature* 411(6834):207–211.
40. Camenisch TD, Koller BH, Earp HS, Matsushima GK (1999) A novel receptor tyrosine kinase, Mer, inhibits TNF-alpha production and lipopolysaccharide-induced endotoxic shock. *J Immunol* 162(6):3498–3503.
41. Tibrewal N, et al. (2008) Autophosphorylation docking site Tyr-867 in Mer receptor tyrosine kinase allows for dissociation of multiple signaling pathways for phagocytosis of apoptotic cells and down-modulation of lipopolysaccharide-inducible NF-kappaB transcriptional activation. *J Biol Chem* 283(6):3618–3627.
42. Rothlin CV, Ghosh S, Zuniga EI, Oldstone MB, Lemke G (2007) TAM receptors are pleiotropic inhibitors of the innate immune response. *Cell* 131(6):1124–1136.
43. Eken C, et al. (2010) Ectosomes released by polymorphonuclear neutrophils induce a MerTK-dependent anti-inflammatory pathway in macrophages. *J Biol Chem* 285(51):39914–39921.
44. Cumpelik A, Ankli B, Zecher D, Schifferli JA (2015) Neutrophil microvesicles resolve gout by inhibiting C5a-mediated priming of the inflammasome. *Ann Rheum Dis*.
45. Wallet MA, et al. (2008) MerTK is required for apoptotic cell-induced T cell tolerance. *J Exp Med* 205(1):219–232.
46. McColl A, et al. (2009) Glucocorticoids induce protein S-dependent phagocytosis of apoptotic neutrophils by human macrophages. *J Immunol* 183(3):2167–2175.
47. A-Gonzalez N, et al. (2009) Apoptotic cells promote their own clearance and immune tolerance through activation of the nuclear receptor LXR. *Immunity* 31(2):245–258.
48. Heo KS, et al. (2014) ERK5 activation in macrophages promotes efferocytosis and inhibits atherosclerosis. *Circulation* 130(2):180–191.
49. Beil WJ, Meinardus-Hager G, Neugebauer DC, Sorg C (1992) Differences in the onset of the inflammatory response to cutaneous leishmaniasis in resistant and susceptible mice. *J Leukoc Biol* 52(2):135–142.
50. Lagrota-Candido J, et al. (2010) Characteristic pattern of skeletal muscle remodelling in different mouse strains. *Int J Exp Pathol* 91(6):522–529.
51. Freire MO, Van Dyke TE (2013) Natural resolution of inflammation. *Periodontol 2000* 63(1):149–164.
52. Bell JH, Herrera AH, Li Y, Walcheck B (2007) Role of ADAM17 in the ectodomain shedding of TNF-alpha and its receptors by neutrophils and macrophages. *J Leukoc Biol* 82(1):173–176.
53. Tsou WI, et al. (2014) Receptor tyrosine kinases, TYRO3, AXL, and MER, demonstrate distinct patterns and complex regulation of ligand-induced activation. *J Biol Chem* 289(37):25750–25763.
54. Warming S, Costantino N, Court DL, Jenkins NA, Copeland NG (2005) Simple and highly efficient BAC recombineering using galK selection. *Nucleic Acids Res* 33(4):e36.
55. Arnardottir HH, Dalli J, Colas RA, Shinohara M, Serhan CN (2014) Aging delays resolution of acute inflammation in mice: reprogramming the host response with novel nano-proresolving medicines. *J Immunol* 193(8):4235–4244.
56. Flamand N, Luo M, Peters-Golden M, Brock TG (2009) Phosphorylation of serine 271 on 5-lipoxygenase and its role in nuclear export. *J Biol Chem* 284(1):306–313.
57. Markoutsa S, et al. (2014) Analysis of 5-lipoxygenase phosphorylation on molecular level by MALDI-MS. *FEBS J* 281(8):1931–1947.
58. Rådmark O, Werz O, Steinhilber D, Samuelsson B (2007) 5-Lipoxygenase: Regulation of expression and enzyme activity. *Trends Biochem Sci* 32(7):332–341.
59. Colas RA, Shinohara M, Dalli J, Chiang N, Serhan CN (2014) Identification and signature profiles for pro-resolving and inflammatory lipid mediators in human tissue. *Am J Physiol Cell Physiol* 307(1):C39–C54.

Supporting Information

Cai et al. 10.1073/pnas.1524292113

SI Materials and Methods

Generation of Mertk^{CR} Mice. A cleavage-resistant MerTK (MerTK$^{\Delta 483-488}$) vector was generated by a two-step BAC "recombineering" knock-in approach (54). Briefly, by using SW105 cells, the 6-aa/18-nt *Mertk* cleavage site in *Mertk* BAC Clone RP23-466I22 (GenBank accession no. AG580391) was replaced with a temporary selectable marker (galK) via homologous recombination. Positive selection was based on growth in minimal media containing galactose as the only carbon source. The galK expression cassette was flanked by 50-nt regions immediately upstream and downstream of the *Mertk* cleavage site codons (tac gca ccc tcg tca acc), which resides on chromosome 2, exon 10 (NM_008587). Second, the galK cassette was removed by recombination with a 100-bp homologous double-strand oligonucleotide spanning 50 bp on either sides of the *Mertk* cleavage site codons. Removal of the cassette was selected for by resistance to 2-deoxy-galactose, which, when phosphorylated by galK, becomes cytotoxic. After inserting a floxed Neo cassette into the *Mertk*$^{\Delta 483-488}$ BAC, a LNL (Loxp-Neo-Loxp) cassette was inserted into the intron downstream of exon 10. The gene-targeting vector was then generated by inserting into a plasmid a sequence containing 5 kb upstream of the deletion site, the LNL cassette, and the sequence 2 kb downstream of the cassette. This plasmid was then introduced into KV1 ES cells (129S6B6 hybrid) to modify the *Mertk* allele through homologous recombination. A forward primer from the LNL cassette and a reverse primer in the downstream region of the 2-kb short arm (not residing in the short arm) were used for PCR to confirm insertion of the targeted Neo-containing Mertk mutant allele. Another forward primer in the upstream region of the 5-kb long arm and a reverse primer form the LNL cassette were used for PCR, and the PCR product was used to validate the deletion of the codons encoding the 6 amino acids spanning the MerTK cleavage site by DNA sequencing. Targeted ES clones were then injected into C57BL/6J blastocysts to generate germ-line chimeras, which carried agouti coat color contributed by the dominant Agouti allele (A) from KV1 ES cells. To confirm germ-line transmission, male chimeric mice were bred to C57BL/6J female mice such that Agouti F1 pups were indicative of germ-line transmission. The neo cassette was removed by crossing the F1 heterozygotes to EIIa-Cre deleter mice (B6.FVB-Tg [EIIa-cre] C5379Lmgd/J). After the removal of the neo cassette, the heterozygote floxed allele in the pups was further confirmed by PCR genotyping.

Preparation of Murine BMDMs and Human Monocyte-Derived Macrophages. For BMDMs, bone marrow cells were cultured for 7 d in DMEM containing macrophage-colony stimulating factor (21). For human macrophages, monocytes were isolated from buffy coats of de-identified healthy volunteers (New York Blood Center) (55). For differentiation into macrophages, the monocytes were cultured for 10 d in RPMI medium, containing glutamine, penicillin/streptomycin, 10% (vol/vol) FBS, and 10 ng/mL recombinant human GM-CSF (PeproTech).

Flow-Cytometric Assessment of Exudate Cells. Peritoneal exudate cells harvested at the indicated times were washed in FACS-staining buffer [PBS containing 3% (vol/vol) FBS], incubated with Fc block (BD Biosciences) for 5 min at 4 °C, and then labeled with Pacific Blue- Ly6G (clone 1A8, eBioscience) and FITC-F4/80 (eBioscience) or appropriate isotype control IgG for 30 min at 4 °C. For apoptotic PMN analysis, exudate cells were cos-tained with 488-Annexin V (Life Technology) and Pacific Blue-Ly6G for 30 min at 4 °C. For surface MerTK staining, cells were costained with FITC-F4/80 and APC-MerTK (R&D Systems). For assessment of macrophages with internalized PMNs, exudate cells were fixed (BD Cytofix), labeled with FITC-F4/80 for 30 min, permeabilized with 0.1% Triton, and then were labeled with PE-Ly6G (BioLegend) for 30 min (26). For assessment of platelet-leukocyte aggregates (PLAs), 50 μL of whole blood underwent red blood cell lysis using BD PharmLyse (BD) per the manufacturer's instructions (BD PharmLyse). Aliquots of ∼1 × 10^6 cells were re-suspended in FACS buffer containing a mixture of antibodies or isotype controls, which included FITC-CD41 (eBioscience), PerCP Cy5.5-Gr1 (BD Biosciences), PECy7-CD11b (eBioscience), Pacific Blue-CD45 (BioLegend), and APC-CD115 (eBioscience). After 30-min incubation at 4 °C, the cells were centrifuged at 8,000 × g for 5 min and then resuspended in 5% (vol/vol) formalin for overnight fixation. Before analysis, the cells were centrifuged and then resuspended in FACS buffer for analysis. Flow-cytometric assessment was performed by using a FACSCanto II (BD Biosciences), and data were then analyzed by using FlowJo (Tree Star).

ELISA Assays for TGF-β and TNF-α. Levels of TGF-β and TNF-α from mouse peritoneal exudates and plasma were quantified by using platinum ELISA (eBioscience), according to the manufacturer's instructions.

Efferocytosis Assay. Jurkat cells were labeled with Calcein Green-AM and then exposed to UV light (254 nm, UVP) for 5 min to induce apoptosis. The labeled ACs were then added to BMDMs plated on coverslips (LabTek) at a ratio of 5 ACs:1 macrophage. After incubation for 1 h, the percent macrophages with internalized ACs were quantified by fluorescence microscopy (Fig. 2C).

Confocal Microscopy for Intracellular Localization of 5-LOX. BMDMs were plated on coverslips and incubated with either IgG or MerTK-activating antibody, as described in the figure legends. Some of the BMDMs were transfected with plasmids encoding WT-5-LOX or mutant 5-LOX in which Ser-272, which is referred to as Ser-271 in the literature (37, 56–58), was mutated to an aspartic acid residue; for consistency with the literature, we refer to this mutant construct as S271D-5-LOX (11). WT 5-LOX plasmid was purchased from Origene, and mutagenesis was carried out by Genewiz. Transfection of these plasmids was done on fully differentiated BMDMs with JetPei macrophage reagent (Polyplus), using 4.2 μg of plasmids and a transfection time of 48 h. After the addition of 5% (vol/vol) cold formalin, the cells were incubated for 60 min at 4 °C with permeabilization buffer (BD Perm/Wash) containing anti–5-LOX antibody (Abcam). Excess antibody was then removed, and the cells were incubated with Alexa 568 anti-rabbit–IgG (Life Technology) for an additional 30 min at 4 °C. The cells were counterstained with Hoechst to identify nuclei, viewed on a Nikon A1 confocal microscope, and analyzed by using ImageJ software (11).

Cell Fractionation and Immunoblotting. Cytosolic and nuclear fractions from human monocyte-derived macrophages were harvested by using the Nuclear Extract Kit from Active Motif according to the manufacturer's instructions. Cell extracts were electrophoresed on 4–20% gradient SDS-polyacrylamide gels and transferred to 0.45-μm nitrocellulose membranes. The membranes were blocked in Tris-buffered saline/0.1% Tween 20 (TBST) containing 5% (wt/vol) nonfat milk at room temperature for 1 h and then incubated with the primary antibody in TBST containing 5% (wt/vol) nonfat milk or 5% (wt/vol) BSA at 4 °C overnight. The membranes were then in-cubated with the appropriate secondary antibody coupled to

horseradish peroxidase, and proteins were detected by the ECL Supersignal West Pico chemiluminescence kit (Pierce). Antibodies used for immunoblotting were as follows: polyclonal goat anti-mouse MerTK antibody and goat anti-human MerTK antibody (R&D Systems); anti–phospho-MerTK (FabGennix); anti–phospho-5-LOX (S271); anti–5-LOX; anti–phospho-MK2; anti-MK2; anti–phospho-p38 MAPK (Thr-180/Tyr-182), anti-p38 MAPK, anti–phospho-NF-κB, anti–NF-κB, anti-lamin A/C, anti–HRP-GAPDH, and anti–HRP-β-actin (Cell Signaling Technologies).

siRNA Treatment. ON-TARGETplus human MerTK siRNA and negative control RNA were purchased from Dharmacon. Human monocyte-derived macrophages were incubated in medium containing 50 nM siRNA or control RNA plus Lipofectamine RNAiMAX (Life Technology). After 24 h, the media were replaced with fresh media without these reagents. After 48 h, the experiments were conducted as indicated.

Identification and Quantification of Lipid Mediators by LC-MS/MS. The 20-h zymosan exudates or macrophage media were combined with 2 volumes of ice-cold methanol and stored at –80 °C. Internal deuterium-labeled standards, including d_5-RvD2, d_4-LTB$_4$, d_8-5-HETE, d_4-PGE$_2$ and d_5-LXA$_4$, were then added to assess extraction recovery. Solid phase extraction and LC-MS/MS analysis was carried out essentially as described in ref. 59. Briefly, lipid mediators were extracted by C18 column chromatography, and methyl formate fractions were taken to dryness under a stream of N_2 gas before suspension in methanol:water

(50:50). Samples were analyzed by using a high-performance liquid chromatograph (Shimadzu) coupled to a QTrap5500 mass spectrometer (AB Sciex). The instrument was operated in negative ionization mode, and lipid mediators were identified and quantified by using multiple reaction monitoring (MRM) transitions, information-dependent acquisition, and enhanced product ion scanning (59), after normalization to extraction recovery based on internal deuterium-labeled standards and calibration curves using external standards for each mediator. The specific MRM transitions used were: 17-HDHA (343 > 245), 14-HDHA (343 > 205), 5-HETE (319 > 115), 12-HETE (319 > 179), 15-HETE (319 > 219), 12-HHT (279 > 163), 4-HDHA (343 > 101), RvD1 (375 > 121), RvD2 (375 > 175), RvD3 (375 > 147), RvD4 (375 > 101), RvD5 (359 > 199), RvD6 (359 > 101), PGD$_2$ (351 > 189), PGE$_2$ (351 > 175), TxB$_2$ (369 > 169), LTB$_4$ (335 > 195), Δ6-*trans*-LTB$_4$ (335 > 195), 12epi-Δ6-*trans*-LTB$_4$ (335 > 195), 5-HEPE (317 > 115), 5S,15S-diHEPE (333 > 115), 7-HDHA (343 > 141), LXA$_4$ (351 > 115), 15-epi-LXA$_4$ (351 > 115), 12-HEPE (317 > 179), 18-HEPE (317 > 259), PGF$_{2α}$ (353 > 193), 5,15-diHETE (335 > 235), 5S,6R-diHETE (335 > 115), 10S,17S-diHDHDA (359 > 153), 10R,17R-diHDHA (359 > 153), LXB$_4$ (351 > 221), 15-epi-LXB$_4$ (351 > 221), LXB$_4$ isomer (351 > 221), RvE1 (349 > 161), RvE3 (333 > 245) Mar2 (359 > 221) and 4S,14S-diHDHA (359 > 159). To analyze global differences in the lipid mediator metabolomes with respect to genotype for peritonitis studies, we used Metaboanalyst and PLS-DA. For individual graphs, lipid mediators were grouped as indicated in the figure legends.
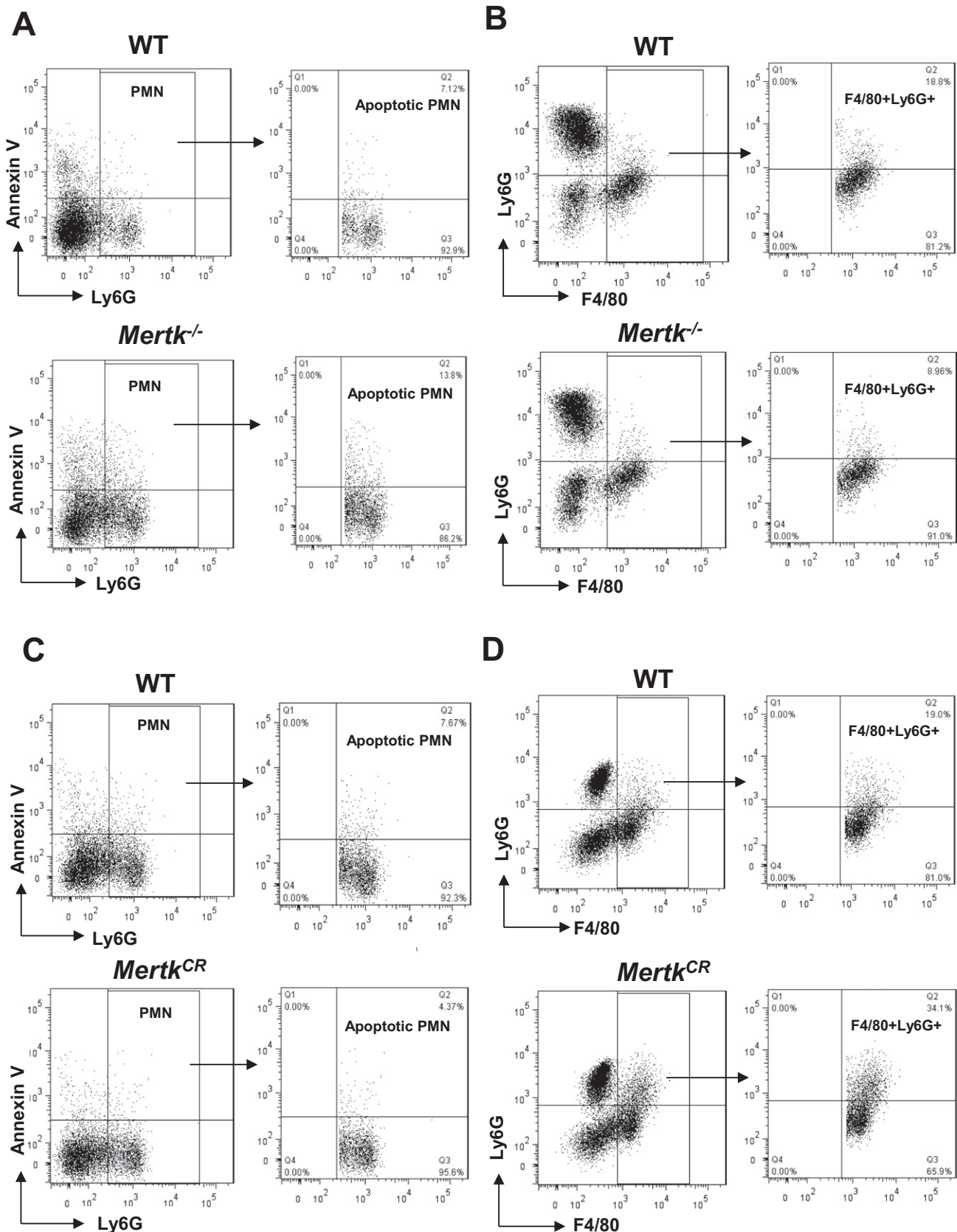
Fig. S1. FACS gating strategy for assessing apoptotic PMNs and efferocytosis in the exudates of zymosan-treated mice. (*A* and *C*) Apoptotic PMNs were assessed by costaining with Annexin V and Ly6G. (*B* and *D*) Apoptotic PMNs engulfed by macrophages were assessed by costaining with F4/80 and Ly6G, as described in Fig. 1 *B* and *C*.
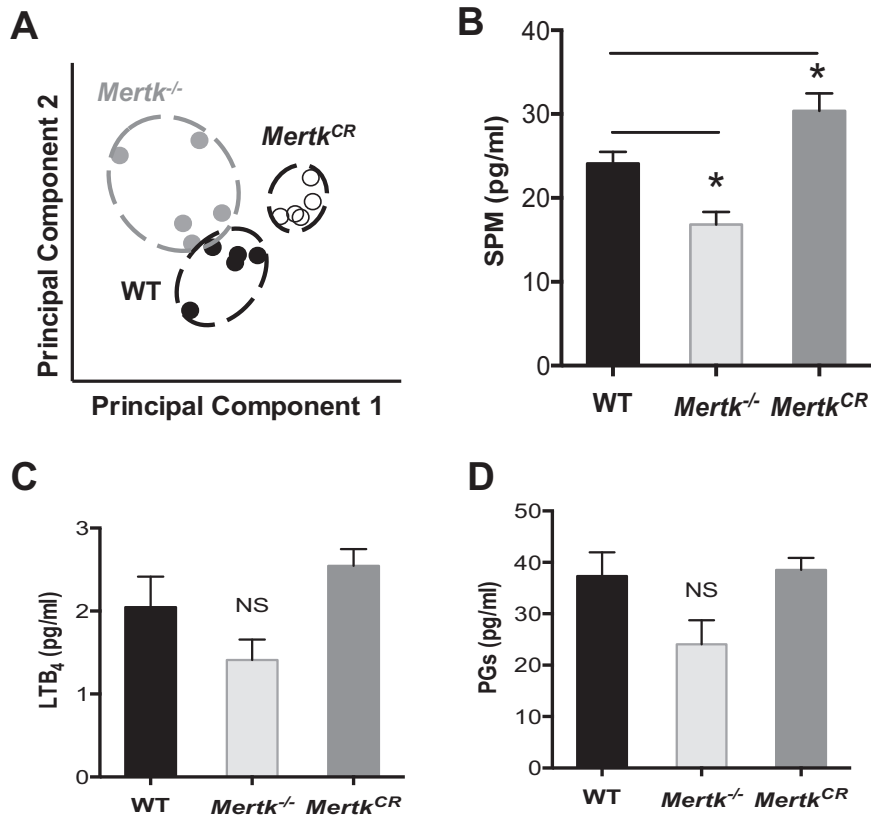
Fig. S2. LC-MS/MS analysis of lipid mediators in WT, *Mertk*^{−/−}, and *Mertk*[CR] mice. (*A*) PLS-DA 2D score plot of lipid mediators measured in peritoneal exudates of WT, *Mertk*^{−/−}, and *Mertk*[CR] mice 20 h after zymosan administration. (*B–D*) Levels of SPMs (RvD1-6, RvE1, RvE3, LXA$_4$, 15-epi-LXA$_4$, LXB$_4$, 15-epi-LXB$_4$, LXB$_4$ isomer, Mar2, 17*R*-PD1 and 10*S*,17*S*-diHDHA), prostaglandins (PGD$_2$, PGE$_2$, and PGF$_{2\alpha}$), and LTB$_4$ in peritoneal exudates 20 h after zymosan administration. Data are mean ± SEM; *n* = 5 mice per genotype. *$P < 0.05$ vs. WT by one-way ANOVA, followed by Dunnett's posttests; ns, not significant.
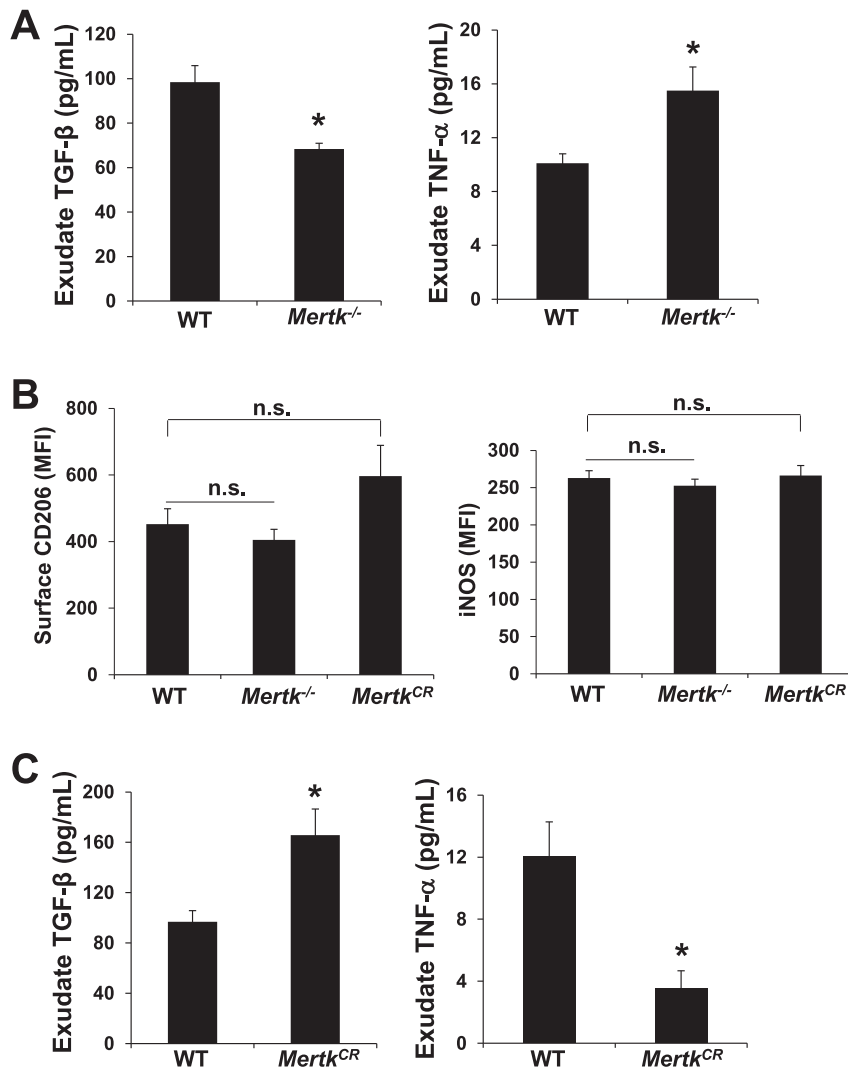
Fig. S3. Exudate TGF-β is decreased and TNF-α is increased in *Mertk*$^{-/-}$ mice, with an opposite effect in *Mertk*^{CR} mice. (*A* and *C*) WT, *Mertk*$^{-/-}$, or Mertk^{CR} mice were injected intraperitoneally with 1 mg of zymosan per mouse. After 30 h, exudate fluid was harvested and subjected to TGF-β and TNF-α measurement by ELISA. (*B*) Expression of cell-surface CD206 and cellular iNOS expression in 30-h exudate F4/80$^+$ macrophages from WT, *Mertk*$^{-/-}$, or Mertk^{CR} mice was quantified by flow-cytometric analysis.
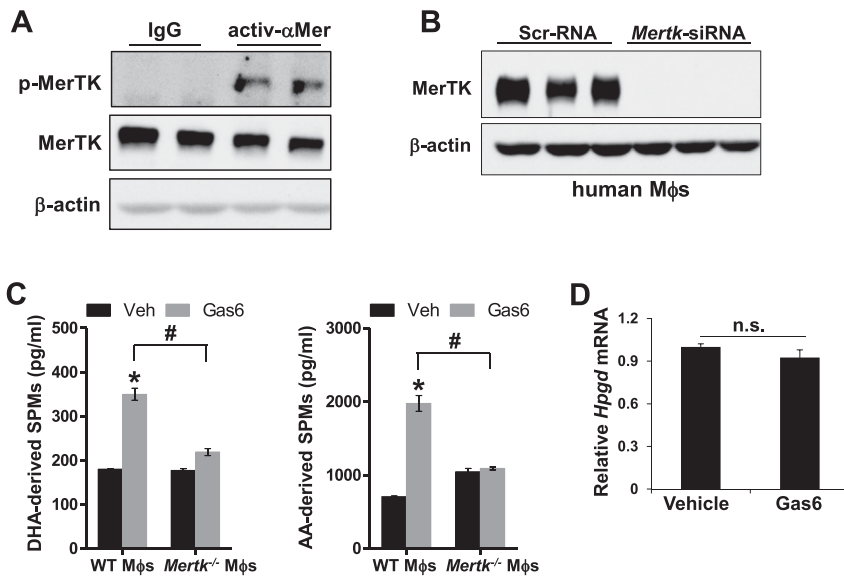
Fig. S4. Validation of activating anti-MerTK antibody and *Mertk* siRNA, and LC-MS/MS analysis of lipid mediators in WT and *Mertk*$^{-/-}$ macrophages. (*A*) BMDMs were incubated for 20 min with 5 nM MerTK-activating antibody (activ-αMer) or control IgG and then assayed for phospho- and total MerTK by immunoblot. (*B*) Human monocyte-derived macrophages were treated with scrambled (Scr) RNA control or siRNA against *Mertk* and then assayed for MerTK by immunoblot. (*C*) Bone marrow-derived WT or *Mertk*$^{-/-}$ murine macrophages treated for 1 h with vehicle control (Veh) or human Gas6 and then assayed by LC-MS/MS for DHA-derived SPMs (RvD1-6, 10S,17S-diHDHDA, 17R-PD1, and their biosynthetic pathway markers, 17-, 7-, and 4-HDHA) and AA-derived SPMs (LXA$_4$, 15-epi-LXA$_4$, LXB$_4$, 15-epi-LXB$_4$, LXB$_4$ isomer, and their biosynthetic pathway marker, 15-HETE). *$P < 0.05$ vs. vehicle control; #$P < 0.05$ between Gas6-treated WT and *Mertk*$^{-/-}$ macrophages (mean ± SEM, $n = 3$/group). (*D*) BMDMs were incubated with Gas6 for 1 h and then assayed by quantitative RT-PCR for *Hpgd* (15-PGDH) mRNA relative to *36B4* mRNA.
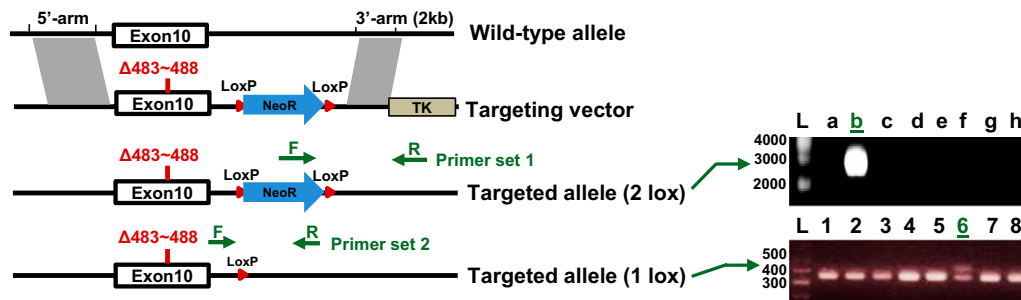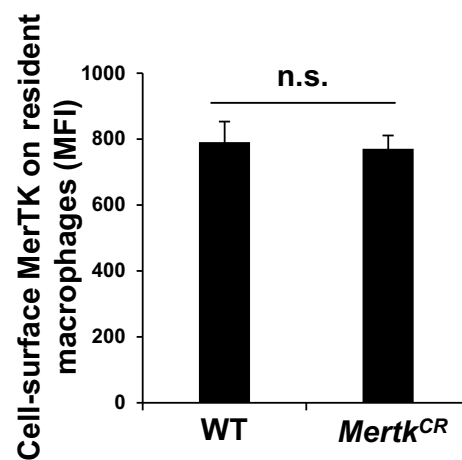

Fig. S5. Design of *Mertk*^{CR} mouse. Diagram shows design of the targeting alleles used to make the *Mertk*^{CR} mouse (see *SI Materials and Methods* for details). The targeting vector contained a mutated version of exon 10 of the Mertk gene in which the codons encoding residues 483–488 of MerTK were deleted and a downstream Neo cassette (NeoR) flanked by *LoxP* sites. ES clones containing this vector via homologous recombination were used to generate germ-line chimeras, which were then bred to EIIa-Cre mice to remove the NEO cassette. (*Upper* gel): Representative panel from PCR screening of 96 ES clones, using primer set 1, to identify the targeted Neo-containing Mertk mutant allele. L = 1 kb plus DNA ladder; ES clone b shows an ES cell clone with the predicted 2,719-bp amplicon for the targeting vector. (*Lower* gel): Representative panel of PCR screen, using primer set 2, of DNA from 18 pups resulting from the cross of male chimeras crossed to EIIa (cre/cre) females. The WT amplicon is 348 bp (lower band), and the targeted Neo-minus Mertk mutant allele (L83) is 431 bp (upper band). A total of three pups were found to carry the L83 locus, including pup 6 as shown. L = Invitrogen 1 kb plus ladder.
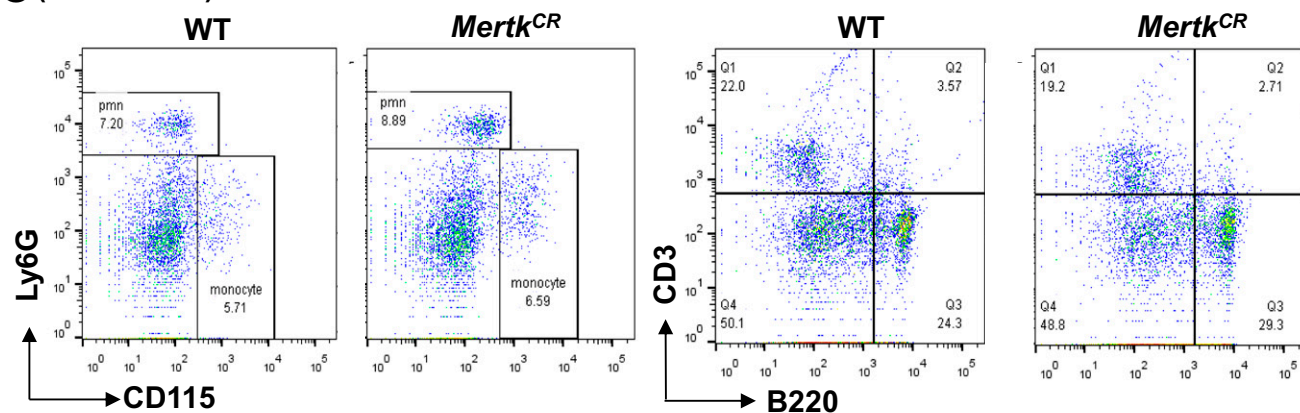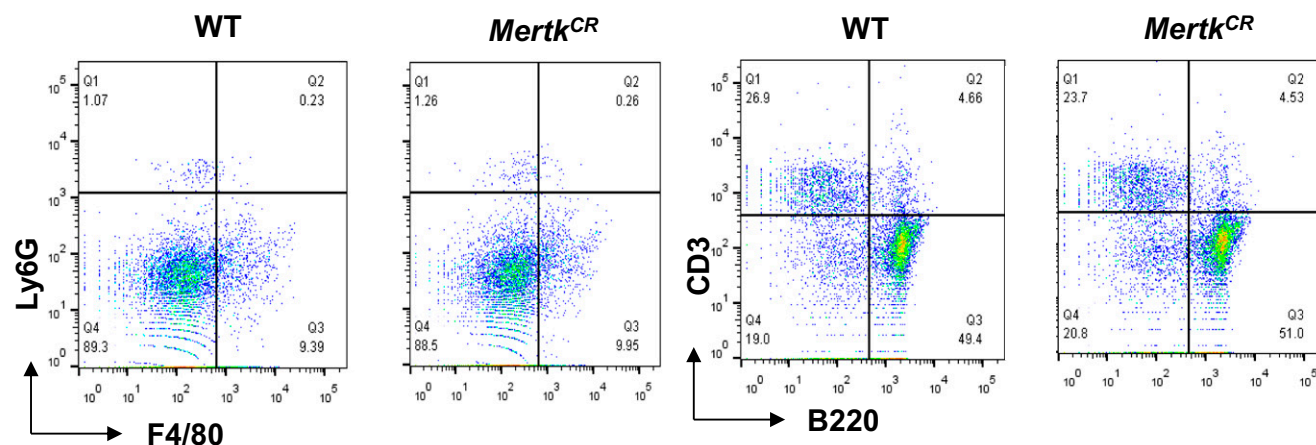
Fig. S6. Macrophage cell-surface MerTK and peripheral immune cells are similar in WT and *Mertk*[CR] mice. (*A*) Resident peritoneal cells from WT and *Mertk*[CR] mice were immunostained for F4/80 and Ly6G and then analyzed by flow cytometry. (*B*) The mean fluorescence intensity (MFI) of cell-surface MerTK on F4/80^{+} cells was quantified by flow cytometry (mean ± SEM, *n* = 4 mice per group; n.s., nonsignificant). (*C* and *D*) WT and *Mertk*[CR] blood and splenic cells were immunostained for Ly6G, CD115, CD3, and B220 antibodies and then analyzed by flow cytometry to detect PMNs, monocytes, T cells, and B cells, respectively.
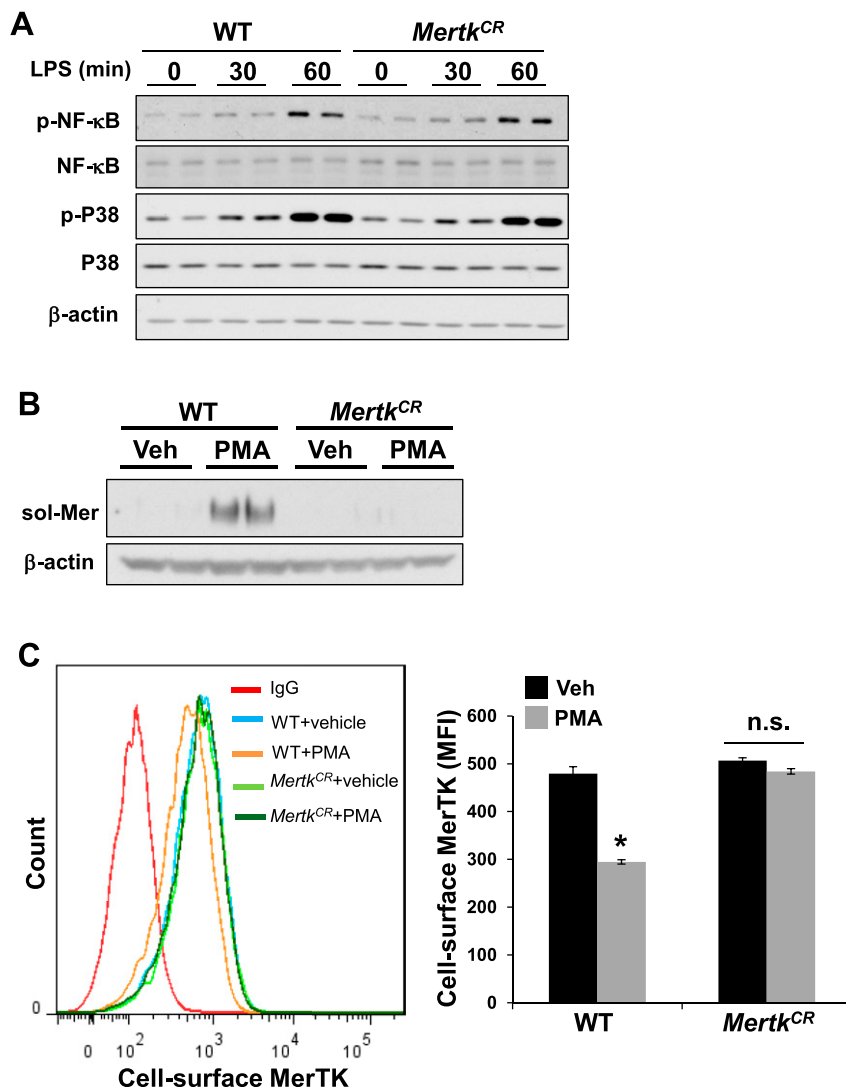
Fig. S7. *Mertk^CR* macrophages respond normally to LPS and are resistant to PMA-induced MerTK cleavage. (*A*) BMDMs from WT or *Mertk^CR* mice were treated with 50 ng/mL LPS for the indicated times and then assayed by immunoblot for phospho- and total NF-κB and P38. (*B*) BMDMs from WT or *Mertk^CR* mice were treated with 50 nM PMA or vehicle control for 2 h, and the media were then assayed for sol-Mer by immunoblot. (*C*) As in *B*, but the cells were analyzed for cell-surface MerTK by flow cytometry. *$P < 0.001$ vs. all other groups (mean ± SEM, $n = 3$ experiments); n.s., nonsignificant.
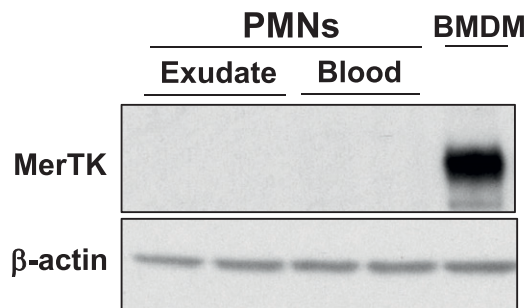

Fig. S8. PMNs do not express MerTK. WT mice were challenged with 1 mg of zymosan intraperitoneally After 4 h, PMNs from either peritoneal exudates or blood were isolated and purified with a PMN purification kit (Miltenyl Biotec). MerTK from purified PMNs was detected by immunoblotting (BMDMs serve as a positive control).
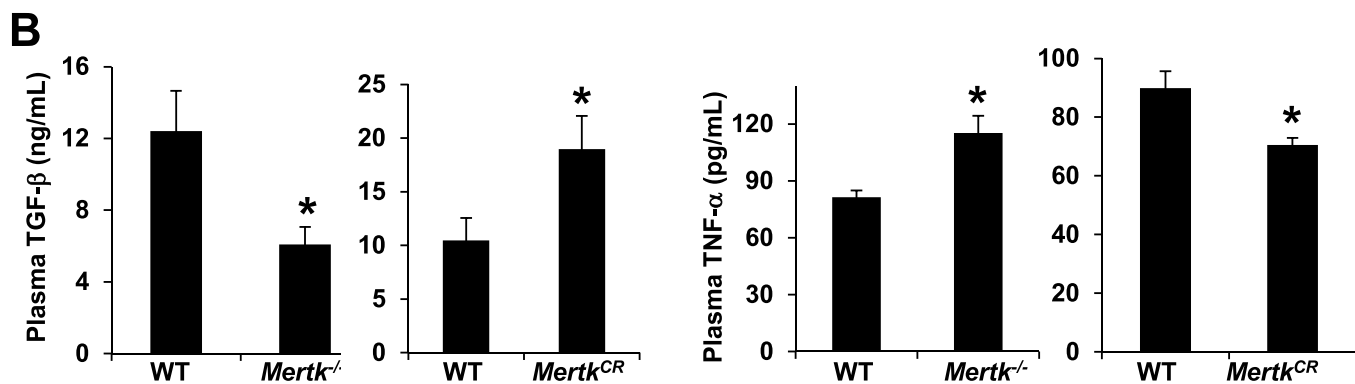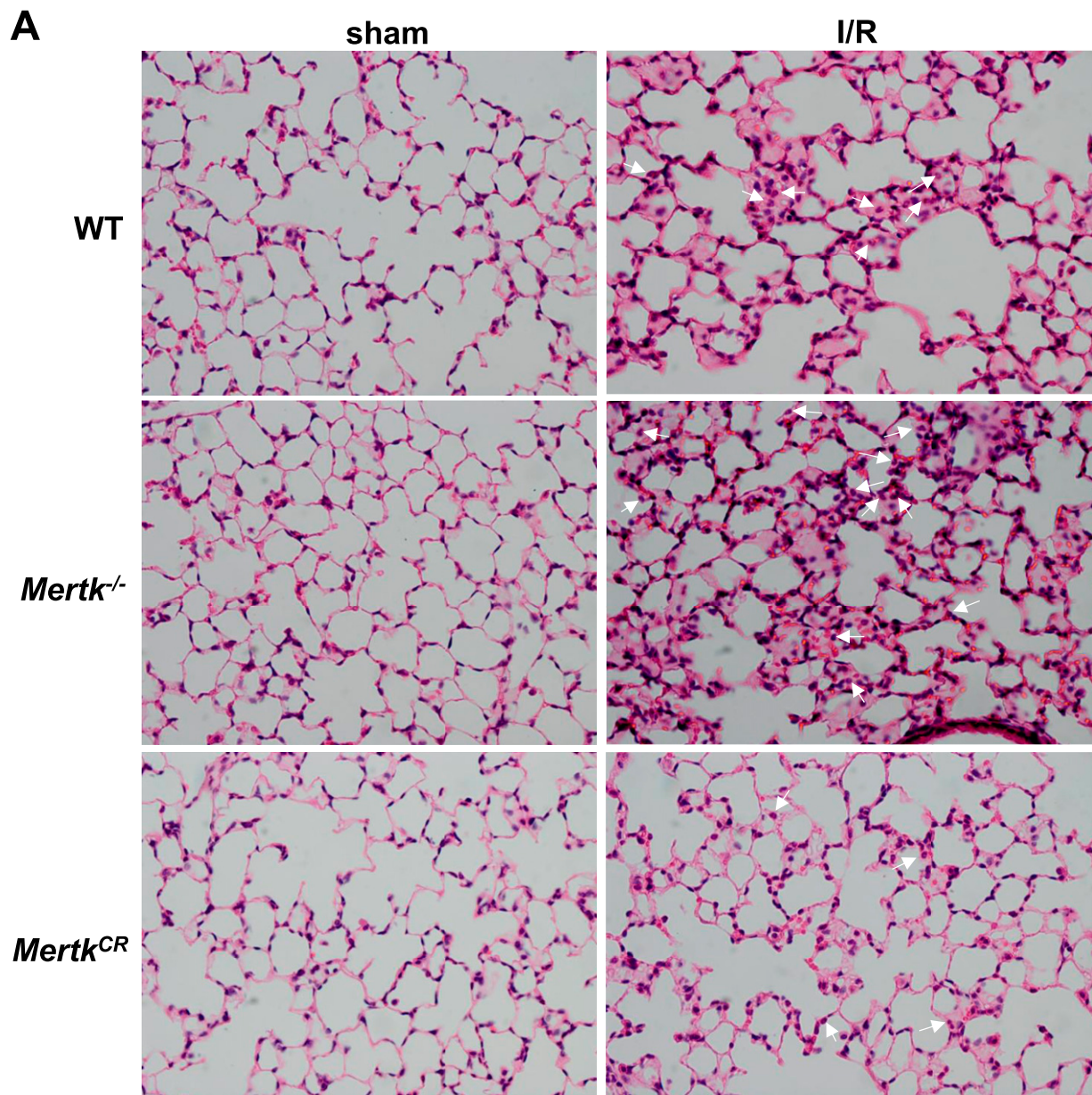
Fig. S9. Hindlimb I/R-induced lung injury is greater in *Mertk*$^{-/-}$ mice and less in *Mertk*^{CR} mice compared with WT mice. (*A*) WT, *Mertk*$^{-/-}$, and *Mertk*^{CR} mice were subjected to 60-min bilateral hindlimb ischemia followed by 120-min reperfusion. Perfused and fixed lungs were then sectioned and stained with hematoxylin and eosin. The quantified lung injury score data appear in Fig. 4*B*. Arrows, neutrophils. (Magnification, 20×.) (*B*) After I/R, plasma TGF-β and TNF-α from WT, *Mertk*$^{-/-}$, and *Mertk*^{CR} mice were measured by ELISA. *$P < 0.05$ vs. WT control mice.
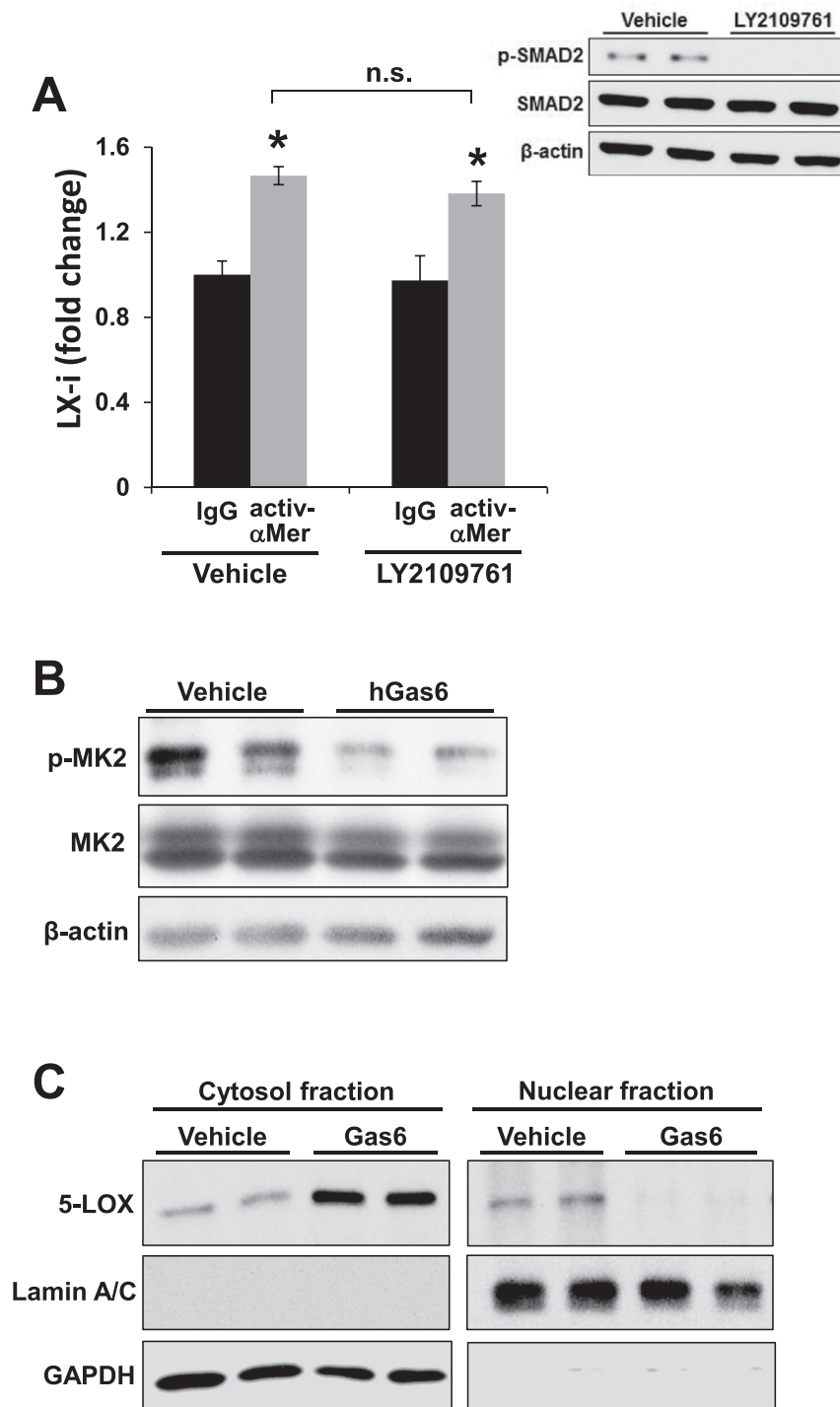
Fig. S10. TGFβ signaling is not involved in MerTK-mediated LX-i synthesis, and MerTK activation reduces phospho-MK2 and enhances cytosol 5-LOX in human monocyte-derived macrophages. (*A*) BMDMs were pretreated with either vehicle or 10 μM LY2109761 (TGF-β receptor inhibitor) for 30 min. Cells were then incubated with either IgG or activ-αMer for 1 h, and the media were collected and assayed for LX-i by ELISA. n.s., nonsignificant. (*A, Inset*) p-SMAD2 immunoblot as a positive control for the inhibitory activity of LY2109761. (*B* and *C*) Human monocyte-derived macrophages were treated for 1 h with vehicle control or human Gas6 and then either immunoblotted for p-MK2 and total MK2 or fractionated into cytosolic and nuclear fractions and immunoblotted for 5-LOX, the nuclear protein lamin A/C, and the cytosolic protein GAPDH.